HEAT FLOW FROM THE EARTH'S INTERIOR: ANALYSIS OF THE GLOBAL DATA SET

Henry N. Pollack
Suzanne J. Hurter[1]
Jeffrey R. Johnson[2]
Department of Geological Sciences
University of Michigan, Ann Arbor

Abstract. We present a new estimate of the Earth's heat loss based on a new global compilation of heat flow measurements comprising 24,774 observations at 20,201 sites. On a 5° × 5° grid, the observations cover 62% of the Earth's surface. Empirical estimators, referenced to geological map units and derived from the observations, enable heat flow to be estimated in areas without measurements. Corrections for the effects of hydrothermal circulation in the oceanic crust compensate for the advected heat undetected in measurements of the conductive heat flux. The mean heat flows of continents and oceans are 65 and 101 mW m^{-2}, respectively, which when areally weighted yield a global mean of 87 mW m^{-2} and a global heat loss of 44.2 × 10^{12} W, an increase of some 4–8% over earlier estimates. More than half of the Earth's heat loss comes from Cenozoic oceanic lithosphere. A spherical harmonic analysis of the global heat flow field reveals strong sectoral components and lesser zonal strength. The spectrum principally reflects the geographic distribution of the ocean ridge system. The rate at which the heat flow spectrum loses strength with increasing harmonic degree is similar to the decline in spectral strength exhibited by the Earth's topography. The spectra of the gravitational and magnetic fields fall off much more steeply, consistent with field sources in the lower mantle and core, respectively. Families of continental and oceanic conductive geotherms indicate the range of temperatures existing in the lithosphere under various surface heat flow conditions. The heat flow field is very well correlated with the seismic shear wave velocity distribution near the top of the upper mantle.

INTRODUCTION

The study of the Earth's conductive heat flux on a global scale allows a greater insight to the internal processes which characterize the Earth's "heat engine" and provides a quantitative measure of the heat content of its exhaust. The heat flow from the interior derives in uncertain proportions from the primordial energy of planetary accretion, the segregation and solidification of the Earth's core, and the decay of radioactive uranium, thorium, and potassium within the Earth. The magnitude of the heat loss is orders of magnitude greater than the energy associated with tidal dissipation, magnetic field generation, seismic strain release, and many other energy fluxes associated with geophysical processes. Accordingly, the determination and description of the regional variations in the global heat flow field is an important endeavor in global geophysics, with special relevance to the tectonics of continents and ocean basins, seismic wave velocities in the Earth's crust and upper mantle, seismicity, rheology, crustal magnetism, hydrothermal circulation within the crust, and the maturation of hydrocarbons, all of which depend strongly on the temperature distribution in the outer few hundred kilometers of the Earth.

In this paper we first review the history of acquisition of terrestrial heat flow data and describe the extensive present-day data compilation. We next present an empirical method of estimating heat flow in unsurveyed areas, leading to a global analysis of the heat flow from continents, oceans, and the Earth as a whole and how the estimates of these quantities have changed as the data set has grown. We then display the heat flow field as a map constructed from the low-degree spherical harmonic components of the global field and compare the harmonic spectrum of the heat flow with the Earth's gravity and magnetic fields and topography. We conclude with a discussion of the implications of the surface heat flow for the temperature structure at shallow depths within the Earth and

[1]Now at Institute of Astronomy and Geophysics, University of São Paulo, São Paulo, Brazil.

[2]Now at Department of Geosciences, University of Arizona, Tucson.

Reviews of Geophysics, 31, 3 / *August 1993*
pages 267–280
8755-1209/93/93RG-01249$15.00
Paper number 93RG01249

TABLE 1. Number of Heat Flow Measurement Sites

Reference	*Continental*	*Oceanic*	*Total*
Birch [1954]	43	20	63
Lee [1963]	73	561	634
Lee and Uyeda [1965]	131	913	1,044
Horai and Simmons [1969]	474	2,348	2,822
Lee [1970]	597	2,530	3,127
Jessop et al. [1976]	1,699	3,718	5,417
Chapman and Pollack [1980]	2,808	4,409	7,217
Chapman and Rybach [1985]	3,601	5,181	8,782
This study	10,337 (13,249)*	9,684 (6,952)*	20,201

*Prior to this paper, measurements in marine waters were usually classified as oceanic. In this table we provide similarly defined numbers but also show in parentheses the breakdown when marine measurements on the continental shelf are classified as being on the continent.

its relationship to seismic shear wave velocity distribution and the thickness of the lithosphere.

THE GLOBAL HEAT FLOW DATA SET

The first continental heat flow measurements were reported by *Bullard* [1939] and *Benfield* [1939], and the first oceanic measurements were reported by *Revelle and Maxwell* [1952]. Only in the last quarter century, however, has the establishment and growth of a global heat flow data set allowed significant geophysical and statistical interpretations of the magnitude and distribution of the heat conducted to the surface of the Earth from its interior. The last comprehensive published compilation of a global data set was by *Jessop et al.* [1976]. The most recent spherical harmonic analysis of heat flow data, performed on the Jessop et al. compilation, was by *Chapman and Pollack* [1975]. *Sclater et al.* [1980] also made use of the Jessop et al. compilation, along with some additional data published subsequently, in a thorough assessment of the Earth's heat loss. Following the Jessop et al. compilation, partial updates and harmonic analyses of the data set [*Chapman and Pollack*, 1980; *Chapman and Rybach*, 1985] were presented and discussed at conferences as the data set grew in size and coverage (see Table 1). The assembly of the present global data set was a project initiated by the International Heat Flow Commission of the International Association of Seismology and Physics of the Earth's Interior to provide a decade update of the Jessop et al. compilation. We believe the present data set to be inclusive of all data published through 1985, but with many subsequently published data also included. Details of the compilation can be found in the appendix.

The present data set includes 24,774 observations. However, it is common for determinations from closely spaced boreholes to be averaged into one site. Accordingly, the averaged value for the cluster is reported first in the data set, followed immediately by data from the individual measurements making up the site average. The data set comprises 20,201 sites so defined; as can be seen from the geographic locations of these sites (Figure 1), the area of coverage of heat flow observations on the Earth's surface in this compilation is nonuniform. More easily accessible or more geologically significant areas tend to have a greater number of measurements than do more inaccessible terrains such as Antarctica and the high-latitude oceans or large regions of Africa and South America. On a 5° grid of the Earth's surface, those grid elements with at least one measurement comprise about 62% of the surface of the Earth (Figure 2), an increase of about 20% over the 1976 compilation. Even after clustering of nearby observations into a site, the data density remains highly variable. On the 5° sampling grid, half the elements that contain observations are represented by seven or fewer measurements. At the other extreme, some detailed surveys have yielded several tens of measurements in a 5° grid element.

The site data are displayed in histograms in Figure 3, both on a global basis and segregated into continents and oceans. We mention in passing that the continental and oceanic distributions appear similar, but we immediately caution the reader that the apparent similarity is misleading; the measurements from many areas of ocean floor with thin or no sediment cover are known to be biased downward systematically by the advective effects of ocean water circulating through the oceanic crust [*Lister*, 1972; *Williams and von Herzen*, 1974; *Sclater et al.*, 1976, 1980; *Anderson et al.*, 1977]. One must also be cautious about making continental and oceanic comparisons or global inferences directly from Figure 3 because of the uneven geographic distribution of measurements, with the attendant possibility of geological bias. Both the hydrothermal and the geographic biases must be addressed in order to achieve reliable estimates of the mean continental, oceanic, and global heat loss. We address these problems by developing empirical estimators of heat flow for unsurveyed or hydrothermally perturbed areas, as is described in the following sections.

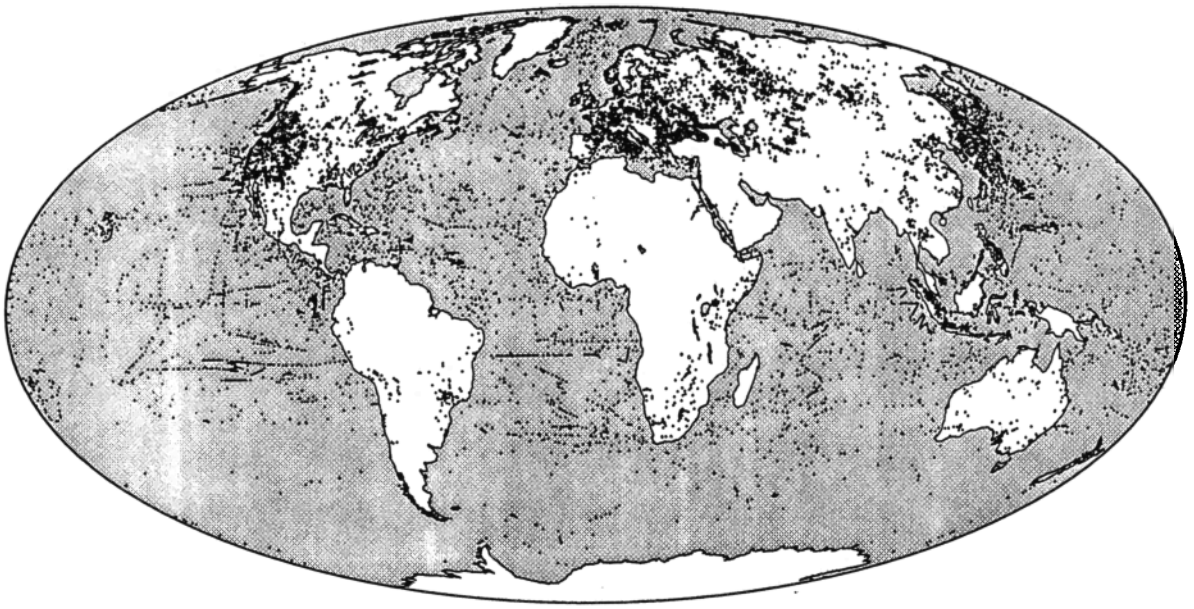

Figure 1. Geographic distribution of heat flow measurement sites.

EMPIRICAL HEAT FLOW ESTIMATORS

Chapman and Pollack [1975] and *Sclater et al.* [1980] used the single criterion of age as the basic parameter for estimating heat flow in areas without measurements. On the continents this was the age of latest tectonothermal mobilization to have affected an area, and in the oceans it was the age of formation of the oceanic crust. The tectonothermal age is typically based on dates from isotopic systems, for instance, K-Ar, Ar-Ar, and Rb-Sr, that have relatively low to moderate closure temperatures. Our estimator is similar in concept to these earlier investigations but differs in application. From the collection of heat flow observations we determine characteristic heat flows for each of the geological units displayed on the map "The bedrock geology of the world" [*Larson et al.*, 1985] and assign these characteristic heat flow values to the geologic units wherever no observations exist. The premise is that similar geologic units should display similar heat flow, a premise supported by the observations for most definitions of geologic similarity.

Twenty-one categories of differing age and geological characteristics, corresponding to the principal mapped subdivisions of *Larson et al.* [1985] (with but one exception, the Precambrian; see below), form the basis of our empirical estimators (see Tables 2 and 3). Each 1° × 1° latitude-longitude grid element on the globe was coded according to the geologic unit indicated on the map at that location. These assignments were made by visually estimating the principal mapped unit in each 1° grid element and inserting the corresponding unit code for that 1° block. In our consideration of various approaches to the coding of the geo-

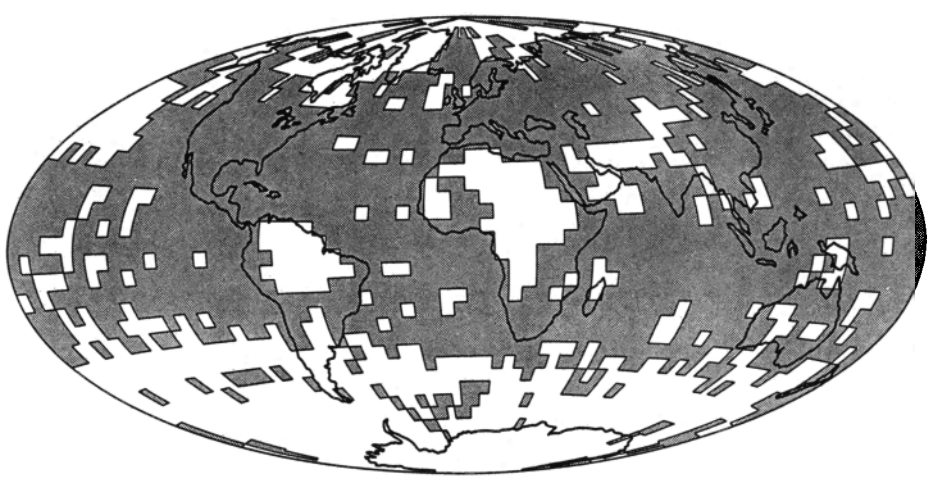

Figure 2. Geographic distribution of heat flow measurements on a 5° × 5° grid; shaded grid elements contain one or more measurements.

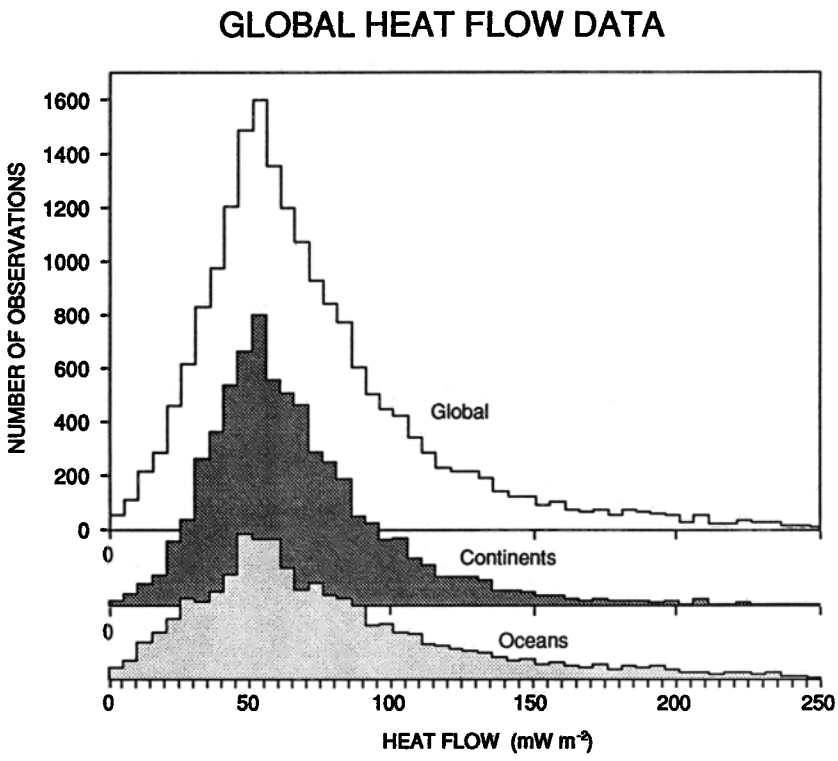

Figure 3. Histograms of heat flow measurements (oceans, continents, and global) grouped by value of measurement.

logical information, the simplicity of assigning a single code to each element outweighed the occasional attendant loss of information in elements where two units appear. At 1° resolution, little error is introduced by this procedure; however, on a 5° grid, as was used by *Chapman and Pollack* [1975], one must areally weight the various geologic units present and carry multiple codes for each grid element. Our principal source of information was the *Larson et al.* [1985] map, but as it covers only latitudes between 71°N and 71°S, polar maps [*Craddock*, 1971; *Herron et al.*, 1974; *Jackson and Gunnarson*, 1990] were utilized to complete the digitization. *Larson et al.* [1985] also group all Precambrian rocks together and do not separate Archean from Proterozoic terrains; however, the *Geological World Atlas* [*Choubert and Faure-Muret*, 1981], which does display Archean regions, enabled a separation of the undivided Precambrian. Table 3 also shows the number of occurrences of each geologic code represented in the global array and in the data set, as well as the area of the Earth covered by each. Each of these codes has been assigned a mean heat flow value (Table 3) based on the observed values contained in the data set. This mean was determined in two steps: first a simple arithmetic averaging of all heat flow values falling in each 1° grid element, and then computation of an areally weighted mean of all grid elements with the same code. The relatively large standard deviations reflect a dispersion of observations in each code similar to that observed in earlier compilations and analyses [*Sclater et al.*, 1980]. However, the large numbers of measurements and of 1° grid elements representing each code yield a small standard error of the heat flow mean determined for each code and allow the means to be used with confidence.

ESTIMATORS IN AREAS AFFECTED BY HYDROTHERMAL CIRCULATION

Several studies [*Lister*, 1972; *Williams and von Herzen*, 1974; *Sclater et al.*, 1976, 1980; *Anderson et al.*, 1977] have demonstrated that circulation of seawater through the oceanic crust is a significant mode of heat transfer in young oceanic regions. Oceanic crust, created at ridges in the process of seafloor spreading, is sufficiently permeable, and the topographic and crustal temperature gradients sufficiently great, to support convective interchange of sea water through the crust for up to tens of millions of years after crustal formation. Conductive heat transfer dominates in older oceanic regions but only after such time as an impermeable sedimentary layer has prevented ocean water interchange with the crust and/or the crustal permeability has been decreased by hydrothermal cementing. The fluid and chemical fluxes within this system are of great interest in their own right, from the perspectives of aqueous chemistry, metallic ore genesis, and the petrology of the oceanic crust [*Rona et al.*, 1983].

The significance of young ocean floor heat transfer processes to the understanding of the global pattern of heat loss is that conductive heat flow measurements seriously underestimate the heat loss on the flanks of active oceanic ridges, a setting occupying about one third of the global surface area. The circulation carries

TABLE 2. Areal Statistics of Map Subdivisions and Data

Map Code	Description	Global		Represented in Data		
		Number of 1° Elements	Area of Earth, %	Number of Observations	Number of 1° Elements	Area of Earth, %
		Oceanic				
1	Cenozoic undifferentiated	1,038	2.2	846	232	0.5
2	Mesozoic undifferentiated	88	0.2	599	49	0.1
3	Quaternary	653	1.2	415	83	0.2
4	Pliocene	1,571	2.4	712	167	0.4
5	Miocene	5,120	9.2	1,211	549	1.3
6	Oligocene	5,152	7.7	593	340	0.7
7	Eocene	5,028	7.8	691	325	0.7
8	Paleocene	2,117	3.9	205	146	0.3
9	Late Cretaceous	3,857	6.9	359	229	0.5
10	Middle Cretaceous	5,641	11.2	695	420	1.0
11	Early Cretaceous	2,609	4.3	331	225	0.5
12	Late Jurassic	1,868	3.8	295	207	0.5
	Oceanic totals	34,742	60.6	9,864	2,972	6.7
		Continental				
13	Subaqueous continental undifferentiated	5,461	9.1	295	731	1.5
14	Cenozoic sedimentary and metamorphic	4,115	8.1	2,912	585	1.5
15	Cenozoic igneous	666	1.1	3,705	134	0.3
16	Mesozoic sedimentary and metamorphic	2,681	4.5	1,359	324	0.8
17	Mesozoic igneous	2,459	1.6	1,591	71	0.2
18	Paleozoic sedimentary and metamorphic	5,126	5.9	403	347	1.0
19	Paleozoic igneous	236	0.4	1,810	29	0.1
20	Proterozoic	7,700	6.2	260	236	0.5
21	Archean	1,544	2.5	963	83	0.2
	Continental totals	30,058	39.4	10,337	2,540	6.1

a significant portion of the crustal heat flux such that the observed value of the conductive heat flow is depressed. Therefore areas affected hydrothermally will show lower conductive heat flow values than would be observed without such effects. The observed conductive heat flow in such areas, i.e., the heat flow that is determined by the marine measurements, must be adjusted upward to be indicative of the true crustal heat flow.

Parsons and Sclater [1977], *Sclater et al.* [1980], and *Stein and Stein* [1992] have shown that in areas where ocean sediments isolate the oceanic crust from ocean water circulation, the heat flow observations are well described by

$$q(t) = Ct^{-1/2} \quad (1)$$

where t is the age of formation of the oceanic crust (in millions of years) at the measurement site, and C is numerically the heat flow in milliwatts per square meter from 1 Ma old crust. The recent analysis by *Stein and Stein* [1992] gives C as 510 mW m^{-2}, an increase of 8% over the estimate by *Parsons and Sclater* [1977]. This inverse relationship between heat flow and the square root of crustal age is exactly of the form predicted by theory for the one-dimensional conductive cooling of a region losing heat through its upper boundary. The relation continues until a time when the effects of conditions at an internal boundary, for example, the base of the lithosphere, affect the solution, at which time oceanic observations began to depart from the simple form given by equation (1) and must be described by a different relationship [see *Stein and Stein*, 1992]. This departure occurs at 65 ± 10 Ma (C. Stein and S. Stein, Constraints on hydrothermal heat flux through the oceanic lithosphere from global heat flow, submitted to *Journal of Geophysical Research*, 1993), an age approximately equivalent to the Cenozoic-Mesozoic boundary. Inasmuch as the circulation of water through the oceanic crust is largely confined to Cenozoic age ocean floor, (1) is a good representation of what the conductive heat flow would be in Cenozoic crust in the absence of the advective perturbation. We therefore use values derived from (1) in place of the empirical means of the data set to provide estimators for such hydrothermally perturbed areas. The estimators are determined for the six affected units by integrating (1) over the appropriate age intervals as shown in Table 3:

TABLE 3. Mean Heat Flow Values for Empirical Predictors

Map Code	Description	Mean Heat Flow, mW m^{-2}		Standard Deviation, mW m^{-2}	Standard Error, mW m^{-2}	Age Range, Ma	
		Observed	Stein and Stein, [1992]				
			Oceanic				
1	Cenozoic undifferentiated	89.3	125.2	43.7	2.8	0.0	66.4
2	Mesozoic undifferentiated	44.6	51.0	22.2	2.8	66.4	245.0
3	Quaternary	*139.5**	*806.4**	93.4	10.1	0.0	1.6
4	Pliocene	*109.1**	*286.0**	81.2	5.9	1.6	5.3
5	Miocene	*81.9**	*142.2**	55.5	2.3	5.3	23.7
6	Oligocene	*62.3**	*93.4**	39.9	2.2	23.7	36.6
7	Eocene	*61.7**	*75.7**	29.3	1.6	36.6	57.8
8	Paleocene	*65.1**	*65.1**	34.3	2.8	57.8	66.4
9	Late Cretaceous	61.5	60.0	31.5	2.1	66.4	84.0
10	Middle Cretaceous	56.3	53.9	21.8	1.0	84.0	119.0
11	Early Cretaceous	53.0	50.5	21.6	1.4	119.0	144.0
12	Late Jurassic	51.3	49.4	16.9	1.2	144.0	163.0
			Continental				
13	Subaqueous continental undifferentiated	77.7		53.6	1.9		
14	Cenozoic sedimentary and metamorphic	63.9		27.5	0.9		
15	Cenozoic igneous	97.0		66.9	5.6		
16	Mesozoic sedimentary and metamorphic	63.7		28.2	1.3		
17	Mesozoic igneous	64.2		28.8	3.0		
18	Paleozoic sedimentary and metamorphic	61.0		30.2	1.2		
19	Paleozoic igneous	57.7		20.5	2.6		
20	Proterozoic	58.3		23.6	1.4		
21	Archean	51.5		25.6	2.4		

*For map codes representing Cenozoic ocean floor, the observed mean values shown in italics are replaced with preferred values from *Stein and Stein* [1992], also shown in italics, which better represent heat flow in regions affected by hydrothermal circulation. The statistics shown refer to the observed heat flow.

$$\bar{q} = (t_2 - t_1)^{-1} \int_{t_1}^{t_2} q(t)\, dt \qquad (2)$$

where $\bar{q}$ is the average heat flow value from oceanic crust with age bounds of t_2 and t_1, and $q(t)$ is given by (1), with $C = 510$ mW m^{-2} as given by *Stein and Stein* [1992]. The values for the affected units are italicized in Table 3. Stein and Stein's analysis enables estimates of heat flow for older ocean floor as well, and these are included for reference in Table 3, although not used as estimators. They are very similar to the mean values we have determined from the data set.

ESTIMATE OF GLOBAL HEAT LOSS

The global heat loss is of significance because it represents the integrated exhaust of the Earth's heat engine and thus is an important constraint that models of the thermal convection within the Earth must accommodate. From the characteristic heat flows and areas represented by each map code (Tables 2 and 3), one can determine the heat loss through each mapped unit as well as the aggregate heat loss through several. We sum separately the contributions of the oceanic and continental terrains and calculate a mean heat flow for oceans and continents of 101 ± 2.2 and 65 ± 1.6 mW m^{-2}, respectively. These values, when weighted by their respective areas, yield a mean global heat flow of 87 ± 2.0 mW m^{-2}, or a global heat loss of 44.2 × 10^{12} W. The uncertainties represent areally weighted standard errors of the mean. Of this heat loss, 70% is lost in the oceans and 30% from the continents, a fact reflecting both the greater area and higher mean heat flow from the oceanic lithosphere. Oceanic lithosphere of Cenozoic age arrayed about the ocean ridge system represents only a third of the Earth's surface but yields over half the global heat loss. The mean heat flow and integrated heat loss we report here exceed earlier estimates for both continents and oceans [*Williams and von Herzen*, 1974; *Davies*, 1980; *Sclater et al.*, 1980]. Accordingly, our estimate of the global heat loss also exceeds earlier estimates, by some 4–8%. This increase is not dramatic and requires no fundamental rethinking of mantle heat transfer systems; the magnitude is less than half of the natural fluctuation in heat loss thought to have occurred over the past 180 m.y. [*Sprague and Pollack*, 1980]. Table 4 shows the vari-

TABLE 4. Continental and Oceanic Mean Heat Flow and Global Heat Loss

	Heat Flow, mW m^{-2}			*Global Heat Loss, 10^{12} W*
	Continental	*Oceanic*	*Global*	
Williams and von Herzen [1974]	61	93	84	42.7
Davies [1980]	55	95	80	41.0
Sclater et al. [1980]	57	99	82	42.0
This study	65 ± 1.6	101 ± 2.2	87 ± 2.0	44.2 ± 1.0

ous earlier estimates of several authors; direct comparisons should be made with a modicum of caution, as each estimate embodies different definitions and values for continental and oceanic areas.

SPHERICAL HARMONIC REPRESENTATION

We now turn to the analytical representation and display of the global heat flow field. The choice of basis functions with which to represent distributions on a sphere is somewhat arbitrary; we have chosen to represent the long-wavelength variability of the heat flow field with a spherical harmonic expansion to degree and order 12. Other choices of basis functions, for example, the harmonic spline approach of *Parker and Shure* [1982], which places primary emphasis on the smoothness of the representation, are attractive in special circumstances such as mapping magnetic field components on the Earth's core. However, smoothness is not the principal concern in representing the surface heat flow; moreover, several geopotential and other fields with which we wish to make spectral comparisons continue to be represented by spherical harmonics, and therefore the comparisons can be most easily made if the heat flow field is similarly represented.

In performing a spherical harmonic analysis of the heat flow data, two approaches can be pursued: (1) represent the observed heat flow at each geographic site as a finite series of spherical harmonics with unknown coefficients and create an overdetermined system of equations to be solved for the coefficients, or (2) analyze a complete data set over the entire globe, determining a finite number of coefficients by direct integration over the sphere. The former method, employed by *Lee and Uyeda* [1965], operates only on the point observations but yields coefficients that are biased by the uneven geographic distribution of the data and which in turn yield unrealistic distortions of the heat flow field in areas unrepresented and therefore unconstrained by data. The latter method, first employed by *Chapman and Pollack* [1975], avoids unrealistic distortions but requires reasonable estimates of heat flow in unsurveyed areas to complement the observed data set and enable integration over the sphere. Here we follow the latter approach because we have already developed empirical estimators of heat flow for unsurveyed areas for the purpose of determining the mean heat flow of continents and oceans and the Earth as a whole. Those estimates, along with the observations where they exist, then constitute a full global array of heat flow data that can be subjected to a spherical harmonic representation free of distortion arising from the irregular distribution of observations. We represent the heat flow field analytically by a surface harmonic expansion of the form

$$q(\theta, \phi) = \sum_{n=0}^{N} \sum_{m=0}^{n} [A_{nm} \cos (m\phi) + B_{nm} \sin (m\phi)] P_{nm}(\cos \theta) \quad (3)$$

where q is the heat flow field, θ is colatitude, ϕ is longitude, A_{nm} and B_{nm} are the coefficients of the expansion, and P_{nm} (cos θ) are the associated Legendre functions fully normalized so that

$$\int_0^{2\pi} \int_0^{\pi} [P_{nm}(\cos \theta) \sin (m\phi)]^2 \sin \theta \, d\theta \, d\phi = 4\pi$$

$$\int_0^{2\pi} \int_0^{\pi} [P_{nm}(\cos \theta) \cos (m\phi)]^2 \sin \theta \, d\theta \, d\phi = 4\pi$$

The harmonic coefficients A_{nm} and B_{nm} were calculated by numerical integration over the sphere as follows:

$$A_{nm} = \frac{1}{4\pi} \int_0^{2\pi} \int_0^{\pi} \bar{q}(\theta, \phi) P_{nm} (\cos \theta) \cdot \cos (m\phi) \sin \theta \, d\theta \, d\phi$$

$$B_{nm} = \frac{1}{4\pi} \int_0^{2\pi} \int_0^{\pi} \bar{q}(\theta, \phi) P_{nm} (\cos \theta) \cdot \sin (m\phi) \sin \theta \, d\theta \, d\phi \quad (4)$$

where $\bar{q}$ is the mean heat flow for a 5° × 5° grid element. The fully normalized coefficients up to degree and order 12 are listed in Table 5, and the synthesized harmonic representation of the global field (equation (3)) shown in Figure 4. The characteristic wavelength represented by a harmonic of degree n is given by the rule of thumb $\lambda \cong 40 \times 10^3$ km/n. Thus the field in

TABLE 5. Harmonic Coefficients of Global Heat Flow Field

n	m	A_{nm}, $mW\ m^{-2}$	B_{nm}, $mW\ m^{-2}$
0	0	86.674	
1	0	−12.999	
1	1	−2.689	−10.417
2	0	−1.971	
2	1	4.578	1.022
2	2	−14.076	6.507
3	0	7.112	
3	1	−2.934	3.555
3	2	7.232	−3.295
3	3	10.299	4.646
4	0	−3.511	
4	1	2.778	−1.873
4	2	1.728	−2.546
4	3	−4.822	.486
4	4	4.408	−17.946
5	0	5.316	
5	1	−1.984	−2.624
5	2	2.167	3.835
5	3	4.570	−6.087
5	4	−8.353	10.283
5	5	−6.896	−4.199
6	0	−5.204	
6	1	2.759	3.162
6	2	2.065	−2.889
6	3	−2.740	−0.252
6	4	−0.012	−1.897
6	5	0.637	0.476
6	6	3.739	7.849
7	0	2.010	
7	1	0.912	0.116
7	2	−6.044	−0.179
7	3	4.999	−0.123
7	4	−1.605	−3.721
7	5	−0.334	3.466
7	6	−4.111	−0.639
7	7	4.126	−1.659
8	0	2.621	
8	1	−1.376	1.795
8	2	7.201	1.436
8	3	−1.947	0.679
8	4	0.204	1.171
8	5	1.851	1.771
8	6	3.579	−0.250
8	7	1.886	4.903
8	8	−5.285	−4.412
9	0	−0.211	
9	1	3.140	0.886
9	2	−1.360	−3.849
9	3	−3.004	−2.056
9	4	1.947	−2.511
9	5	0.328	−3.064
9	6	1.030	−0.745
9	7	−4.117	−3.888
9	8	6.529	3.889
9	9	−4.084	−0.082
10	0	2.735	
10	1	−1.624	−1.998
10	2	−1.309	1.333
10	3	4.576	0.641
10	4	−4.506	0.927
10	5	−0.363	−0.972
10	6	−4.528	−1.353
10	7	−0.952	1.810
10	8	−1.104	−0.739
10	9	0.129	0.644
10	10	4.164	−3.463
11	0	−1.708	
11	1	0.429	2.902
11	2	2.106	0.915
11	3	−5.078	0.595
11	4	3.441	0.907
11	5	0.784	2.762
11	6	0.158	0.782
11	7	−0.377	−0.355
11	8	−0.818	1.851
11	9	3.645	1.336
11	10	−1.765	4.245
11	11	−0.505	−3.520
12	0	1.003	
12	1	−0.689	−1.476
12	2	−2.359	−0.066
12	3	3.863	0.504
12	4	0.793	−1.034
12	5	−1.761	−0.267
12	6	2.439	−2.484
12	7	−2.080	3.714
12	8	2.237	0.809
12	9	0.289	−0.838
12	10	1.516	−4.821
12	11	4.114	−0.553
12	12	−3.033	2.175

Figure 4 comprises wavelengths greater than about 3000 km.

As can be seen from (4), the coefficient A_{00} represents the mean value of the global field. By subtracting it from the field, one can obtain a representation of the deviations from the mean field, displayed in Figure 5 simply as areas above and below the mean. From both Figures 4 and 5 one clearly sees the role of the mid-ocean ridges as heat corridors or heat "leaks" from the Earth's interior; fully half of the Earth's heat loss takes place from the cooling of oceanic lithosphere formed in the Cenozoic. Geographic characteristics immediately apparent are the higher heat flow of the southern hemisphere and the strong longitudinal grain arising from the north-south orientation of much of the ocean ridge system. In the terminology of spherical harmonics, the hemispherical asymmetry is represented principally by the first three odd zonal harmonics ($n = 1, 3, 5$; $m = 0$), and the longitudinal grain by the low-degree sectoral harmonics ($m = n$). As can be seen in Table 5, the contribution of the sectoral coefficients in each of degrees 2, 3, 4, and 6 exceed the contributions of all the other coefficients of same degree.

The harmonic spectrum, defined as $[\sum_m (A_{nm}^2 + B_{nm}^2)/(2n + 1)]^{1/2}$ for each of the degrees, is simply the rms amplitude of all the harmonic coefficients of a given degree. This spectrum is shown in Figure 6, and generally shows declining strength with increasing degree. The two modest peaks at $n = 4$ and 8 reflect the

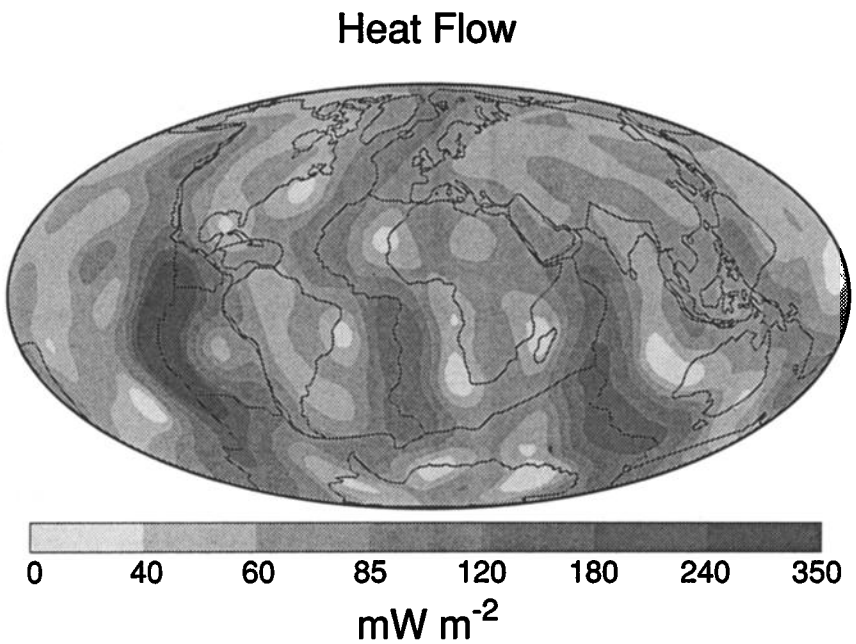

Figure 4. Degree 12 spherical harmonic representation of global heat flow.

approximate 90° separation of the zones of above average heat flow shown in Figure 5.

Comparisons can be drawn between the heat flow spectrum and other global distributions such as topography and the gravitational and magnetic fields, all of which have been analyzed in terms of spherical harmonics [*Balmino et al.*, 1973; *Marsh et al.*, 1990; *Langel*, 1992]. In Figure 7 we display these four spectra in nondimensional form, each having been normalized to unity for the rms amplitude of the lowest harmonic degree present in each spectrum (degree 0 for heat flow, topography, and gravity, and degree 1 for the magnetic field). The absence of degree 1 representation in the gravitational field arises from the fact that with a coordinate system origin at the center of mass, all degree 1 coefficients are identically zero; the degree 2 strength shown includes only the residual nonhydrostatic contribution after removal of the large variation associated with the hydrostatic ellipsoid. The spectra in Figure 7 have been offset from one another for clarity.

The principal feature we call attention to in Figure 7 is the increasingly steep decline in spectral strength with increasing harmonic degree ("reddening") as one progresses from the heat flow and topography to the gravitational and magnetic fields. The simplest interpretation of this progressive increase in the rate of spectral reddening is a linkage to the source depth of the respective fields. The Earth's dominant topography, that is, continents and ocean basins and the oceanic ridge system within the ocean basins, has shallow petrological, tectonic, and thermal origins; the amplitude of dynamic topography [*Cazenave and Lago*, 1991] arising from deeper mantle convection is too small to affect the topographic spectrum significantly. Similarly, the pattern of heat flow is governed by shallow crustal and lithospheric processes. The spectrum of the gravitational field, by contrast, likely

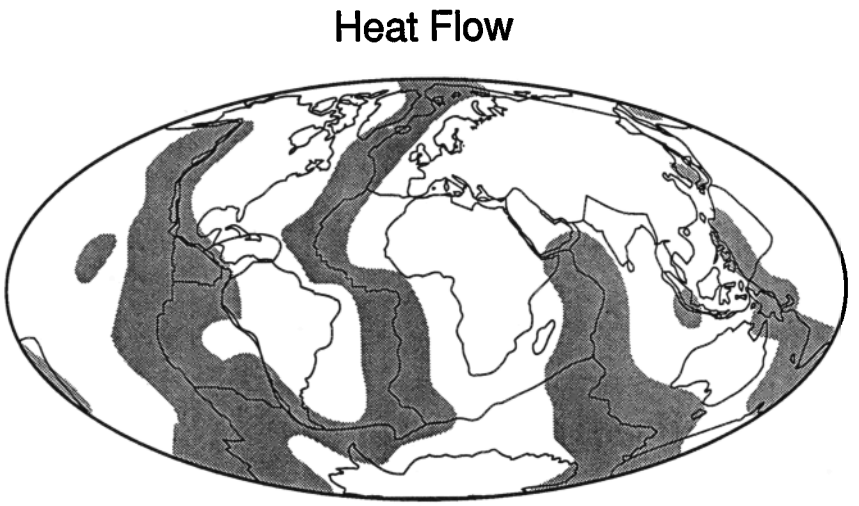

Figure 5. Degree 12 spherical harmonic representation of deviations from the global mean heat flow. Shaded area above the mean, white area below.

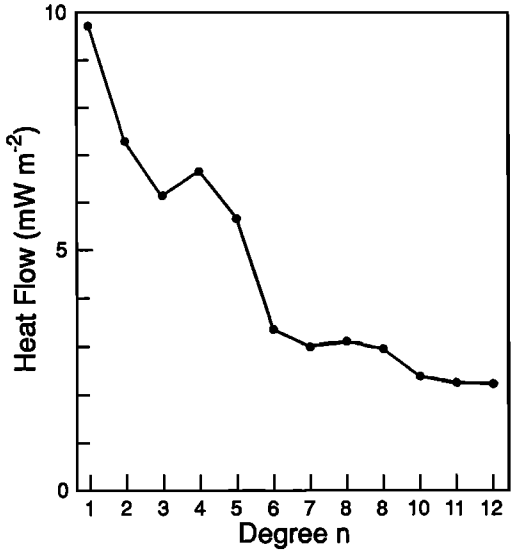

Figure 6. Harmonic spectrum of global heat flow depicted as the rms amplitude of all harmonics of degree n.

draws its low-degree strength principally from the lower mantle [*Hager et al.*, 1985; *Jackson et al.*, 1991]; large density contrasts which exist near or at the Earth's surface, for instance, topography, do not contribute significantly to the long-wavelength components of the geoid because of shallow isostatic compensation. The magnetic field, the most severely reddened of the spectra illustrated, has its source within the Earth's core, at depths obviously greater than all the other fields.

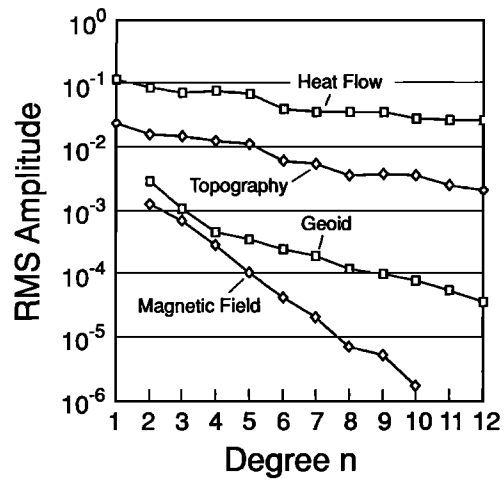

Figure 7. Root-mean-square amplitude of the harmonic spectra of the Earth's topography, heat flow, and gravitational and magnetic fields, normalized to unity at the lowest degree of each field. The spectra of the topography, geoid, and magnetic field as illustrated have been scaled by factors 10^{-1}, 10^{+3}, and 10^{-2} respectively to eliminate overlap and achieve clarity.

IMPLICATIONS OF HEAT FLOW FOR LITHOSPHERIC TEMPERATURES

As noted in the introduction, many physical properties of the Earth's crust and upper mantle are strongly temperature dependent. The profile of temperature with depth through a section of lithosphere is in turn strongly coupled to the heat flow. Several authors have addressed the general problem of calculating lithospheric geotherms in oceans and/or continents [*Chapman and Furlong*, 1992; *Denlinger*, 1992; *Pollack and Sass*, 1988; *Chapman*, 1986; *Lachenbruch and Sass*, 1977; *Pollack and Chapman*, 1977; *Chapman and Pollack*, 1977; *Blackwell*, 1971; *Sclater and Francheteau*, 1970; *Clark and Ringwood*, 1964]. Our purpose here is not to analyze geotherm construction in detail, but rather to outline the attendant considerations and call attention to the degrees of freedom in the exercise. We present a characteristic set of continental and oceanic geotherms that illustrate the strong dependence of lithospheric temperatures on heat flow.

The first assumption common to all of the aforementioned models of lithospheric temperatures is that heat transfer is dominantly by conduction. This assumption then leads directly to the heat conduction equation $-\text{div}\ (-K\ \text{grad}\ T) + A = \partial(\rho cT)/\partial t$, where T is temperature, K is thermal conductivity, A is the volumetric heat production rate, ρ is density, c is specific heat, and t is time.

Issues such as the temperature dependence of conductivity (and hence diffusivity), the depth distribution of conductivity and heat sources, transient or steady

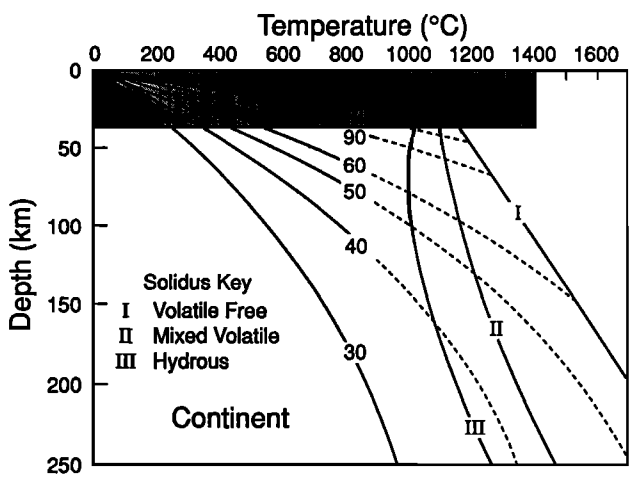

Figure 8. Conductive geotherm family for continental terrains [after *Chapman and Pollack*, 1977; *Pollack and Sass*, 1988]. The number on each geotherm indicates the corresponding surface heat flow in milliwatts per square meter. Generalized solidus curves for peridotite in different volatile environments are also shown. The shaded area above 40 km corresponds to the domain of continental crust. Geotherms are shown with solid lines where conduction is the principal mode of heat transfer and with dashed lines where other modes of heat transfer may have increasing significance.

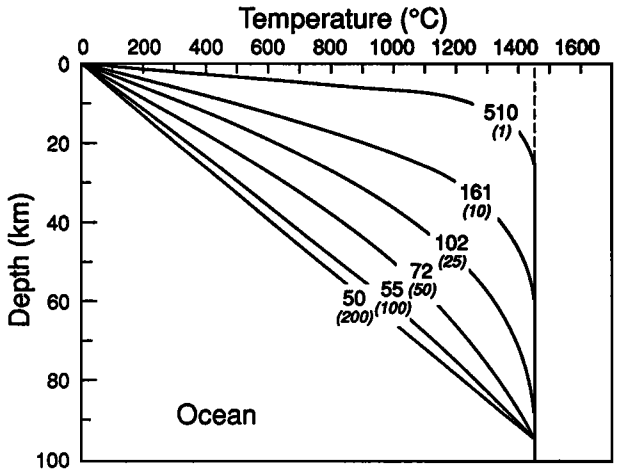

Figure 9. Conductive geotherm family for oceanic lithosphere cooling from initial high temperature, with constant temperature lower boundary condition. Lithospheric thickness is 95 km, initial and lower boundary temperature at 1450°C [after *Stein and Stein*, 1992]. The number on each geotherm indicates the corresponding surface heat flow in milliwatts per square meter parenthetic numbers in italics indicate time in millions of years after beginning of cooling.

state condition, lateral heterogeneity, and the nature of the lower boundary as expressed in the boundary condition must next be addressed. Each has been the subject of numerous papers, many of which can be found in the references cited above. We present in Figures 8 and 9 characteristic geotherms for continental and oceanic lithosphere corresponding to a range of surface heat flow values. The continental geotherms are one-dimensional and steady state and embody temperature dependent conductivity, depth dependent crustal heat sources and uniform mantle heat sources; no explicit lower boundary has been defined, but various melting relations are indicated to call attention to the eventual onset of nonconductive heat transfer. The oceanic geotherms are one-dimensional and time dependent, corresponding to the cooling of a slab of uniform thickness with a fixed temperature at the base of the slab. The values for slab thickness, initial temperature, and physical properties used in the calculation of the oceanic geotherms are those determined by *Stein and Stein* [1992] in their recent analysis of oceanic heat flow and bathymetry.

As a simple illustration of the effect of temperature on physical properties we consider the global distribution of shear wave velocities at 38-km depth, as presented by *Anderson et al.* [1992] and reproduced here in simplified form in Figure 10. The correlation of below average shear wave velocities with above average heat flow (Figure 5) and above average shear wave velocities with below average heat flow is unmistakable. The shear wave velocity variations at that depth are in the range of ±5% about the mean, and given a representative temperature derivative for shear velocity of about -3.5×10^{-4} km s^{-1} °C^{-1} [*Kumazawa and Anderson*, 1969] the range of velocities implies a range of temperatures of approximately 1200°C at that depth. As can be seen from Figures 8 and 9, the geotherm families display such a range at 40 km, and along with the geographic pattern of heat flow offer a compelling explanation for the shear-wave velocity distribution at that depth. Correlation of below average surface heat flow with above average shear wave velocities continues at least to 200 km and perhaps to 400 km beneath the continental cratons [*Su et al.*, 1992], geological units which constitute a thick thermal/chemical boundary layer through which conductive heat transfer dominates. The correlation likely arises because thicker lithosphere offers more thermal resistance to upward and outward bound heat than does thinner lithosphere and therefore leads to a diversion of the deeper advected heat away from the thick lithosphere into regions of thinner lithosphere [*Ballard and Pollack*, 1987; *Nyblade and Pollack*, 1993]. Mid-ocean ridges exhibit the highest heat flow on the globe as well as the thinnest lithosphere; slow shear wave velocities persist beneath ridges to depths of 300 km [*Su et al.*, 1992].

The apparent inverse relationship between heat flow and lithospheric thickness has led to attempts to map lithospheric thickness as an empirical transform

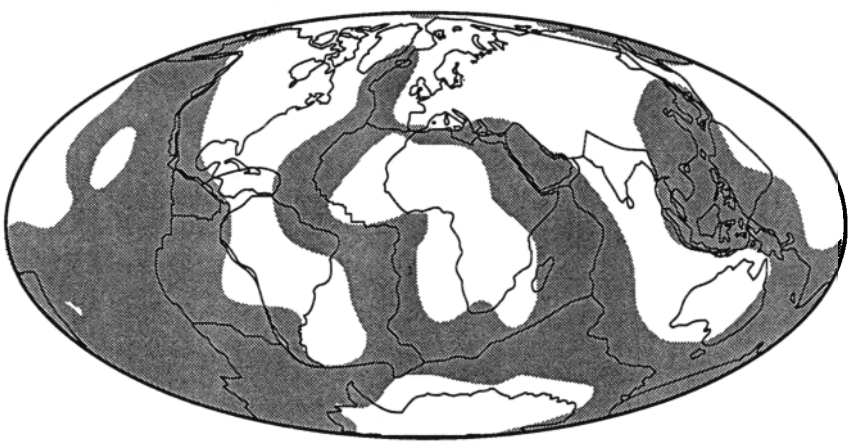

Figure 10. Deviations from the global mean shear wave velocity at 38-km depth (simplified from *Anderson et al.* [1992]). Shaded areas are below the mean; white areas are above.

(nonlinear) of the heat flow field [*Pollack and Chapman*, 1977]. The absolute thickness obtained depends on how the base of the lithosphere is defined. Critical values of temperature, potential temperature, flexural rigidity, viscosity, and shear wave velocity have all been candidates. Below the lithosphere, where presumably convective rather than conductive heat transfer dominates, the relationship between shear wave velocities and the surface heat flow weakens. Heat flow thus can be seen as a useful indicator of thermal conditions principally within the lithosphere; the heat transfer patterns in the deeper interior are increasingly obscure, at least in terms of imparting a robust surface heat flow signature.

APPENDIX

The global heat flow data compilation utilized in this analysis was aided by the efforts of many workers worldwide who compiled initial subsets for: oceanic measurements (K. Louden), Europe (V. Cermak), China (J. Wang and S. Huang), Japan (S. Uyeda), India (M. L. Gupta), South Africa (M. Q. W. Jones), South America and Africa (H. N. Pollack), Canada (A. M. Jessop), and the United States (J. Sass, P. Morgan, and D. Blackwell). These data sets served as foundations for the global set. Additional data, such as those from Australia, were compiled by us from various journals and special publications. These data, along with the *Jessop et al.* [1976] global data set, were combined with the aforementioned subsets through a series of crossreferencing and duplicate checking. This process resulted in numerous editorial alterations among the data subsets as duplicate entries were matched across similar compilations. For example, heat flow values from the Mediterranean Sea were found in both the oceanic and European subsets; comprehensive editing resulted in all Mediterranean Sea values being placed within the European subset.

Occasionally, different heat flow values have been reported for the same site. When the corresponding references for these heat flow values are different as well, only the most recent value has been included in the final compilation. In a few instances, however, the corresponding references are identical. The reason for the discrepancy in the reported heat flow values was often unclear unless the data also provided information on the type of correction applied to the heat flow measurement (see format discussion below). In most such cases, the corrected heat flow value was given priority over the value without any correction.

The data compilation follows closely but not exactly the general format of the *Jessop et al.* [1976] compilation. The actual format utilized is presented in Table A1. In addition to the essential details of the heat flow determination, this format includes (when provided by contributors) codes indicating, for example, the continent or ocean where the measurement was taken or the type of corrections made to the measurements (topography, sedimentation, etc.). Additional information about the measurement provided by the author of the publication, such as uncorrected (raw) heat flow, lithologies encountered, or borehole code names, has in some instances also been included beyond column 80. Users of the data set must bear in mind that the quality and/or reliability of the included data are not uniform. We have attempted to provide as much information as possible about each observation in order to aid users in assessing the quality of each measurement. However, as was stated by *Jessop et al.* [1976, p. 1], "The onus is on the user . . . to make his or her own quality judgement."

TABLE A1. Format of Global Heat Flow Data Compilation Used in This Analysis

Description	*Units*	*Columns*
Data number		1–6
Descriptive codes		7–13
Name of site		15–22
Latitude	deg, min, tenths	23–28
Longitude	deg, min, tenths	29–35
Elevation	m	36–40
Minimum depth	m	41–44
Maximum depth	m	45–48
Number of temperatures		49–51
Temperature gradient	$mK\ m^{-1}$	52–54
Number of conductivities		55–57
Conductivity	$W\ m^{-1}\ K^{-1}$	58–61
Number of heat production		62–64
Heat production	$\mu W\ m^{-3}$	65–68
Heat flow	$mW\ m^{-2}$	69–72
Number of sites		73–74
Reference number		76–77
Year of publication		79–80

The global heat flow data compilation has been turned over the World Data Center A for distribution. Inquiries should be addressed to World Data Center A for Solid Earth Geophysics, NOAA E/GCI, 325 Broadway, Boulder, CO 80303.

The International Heat Flow Commission has appointed E. Hurtig of the GeoforschungsZentrum Potsdam in Germany as the new custodian of the global heat flow data compilation. The maintenance and updating of the data base will be facilitated if authors of publications containing new heat flow observations will send him a manuscript copy or reprint at the following address: Eckart Hurtig, GeoforschungsZentrum Potsdam, Telegrafenberg A 17, D-1561 Potsdam, Germany.

ACKNOWLEDGMENTS. We thank those contributors to the data set mentioned in the text: Keith Louden of Dalhousie University; Vladimir Cermak of the Czech Academy of Science; Wang Jiyang and Huang Shaopeng of the Institute of Geology, Academia Sinica; M. L. Gupta of the National

Geophysics Research Institute of India; M. Q. W. Jones of the University of Witwatersrand; Seiya Uyeda of Tokai University; John Sass of the U.S. Geological Survey; Paul Morgan of Northern Arizona University; and David Blackwell of Southern Methodist University. We also thank Carol Stein and Seth Stein for providing copies of their papers on oceanic heat flow and hydrothermal circulation prior to publication, and Yu-shen Zhang for making available the global distribution of shear wave velocities. David Chapman assisted with the digitization of the geological maps of the polar regions, and Yu-shen Zhang and Yuichiro Tanioka helped prepare the global maps. David Scholl was the editor responsible for this manuscript. Michael Gurnis, Larry Ruff, John Sass, Richard von Herzen, Seiya Uyeda, Geoffrey Vallis, and Alan Chave provided helpful comments which improved the manuscript. This research was supported in part by the U.S. National Science Foundation under grant EAR-8716958. This paper is dedicated to the memory of Francis Birch, who pioneered the measurement of terrestrial heat flow in North America.

REFERENCES

Anderson, D. L., T. Tanimoto, and Y.-S. Zhang, Plate tectonics and hot spots: The third dimension, *Science*, *256*, 1645–1651, 1992.

Anderson, R. N., M. G. Langseth, and J. G. Sclater, The mechanisms of heat transfer through the floor of the Indian Ocean, *J. Geophys. Res.*, *82*, 3391–3409, 1977.

Ballard, S., and H. N. Pollack, Diversion of heat by Archean cratons: A model for southern Africa, *Earth Planet. Sci. Lett.*, *85*, 253–264, 1987.

Balmino, G., K. Lambeck, and W. Kaula, A spherical harmonic analysis of the Earth's topography, *J. Geophys. Res.*, *78*, 478–481, 1973.

Benfield, A. F., Terrestrial heat flow in Great Britain, *Proc. R. Soc. London, Ser. A*, *173*, 428–450, 1939.

Birch, F., The present state of geothermal investigations, *Geophysics*, *19*, 645–659, 1954.

Blackwell, D. D., The thermal structure of the continental crust, in *The Structure and Physical Properties of the Earth's Crust, Geophys. Monogr. Ser.*, vol. 14, pp. 169–184, AGU, Washington, D. C., 1971.

Bullard, E. C., Heat flow in South Africa, *Proc. Roy. Soc. London, Ser. A.*, *173*, 474–502, 1939.

Cazenave, A., and B. Lago, Long wavelength topography, seafloor subsidence and flattening, *Geophys. Res. Lett.*, *18*, 1257–1260, 1991.

Chapman, D. S., Thermal gradients in the continental crust, in The Nature of the Lower Continental Crust, edited by J. B. Dawson et al., *Spec. Publ. Geol. Soc. London*, *24*, 63–70, 1986.

Chapman, D. S., and K. P. Furlong, Thermal state of the continental crust, in *Continental Lower Crust, Dev. Geotecton.*, vol. 23, edited by D. M. Fountain, R. J. Arculus, and R. W. Kay, pp. 179–199, Elsevier, New York, 1992.

Chapman, D. S., and H. N. Pollack, Global heat flow: A new look. *Earth Planet. Sci. Lett.*, *28*, 23–32, 1975.

Chapman, D. S., and H. N. Pollack, Regional geotherms and lithospheric thickness, *Geology*, *5*, 265–268, 1977.

Chapman, D. S., and H. N. Pollack, Global heat flow: Spherical harmonic representation (abstract), *Eos Trans. AGU*, *61*, 383, 1980.

Chapman, D. S., and L. Rybach, Heat flow anomalies and their interpretation, *J. Geodyn.*, *4*, 3–37, 1985.

Choubert, G., and A. Faure-Muret, *Geological World Atlas*, scale 1:10,000,000, UNESCO, Paris, 1981.

Clark, S. P., Jr., and A. E. Ringwood, Density distribution and constitution of the mantle, *Rev. Geophys.*, *2*, 35–88, 1964.

Craddock, C., Geologic map of Antarctica, scale 1:5,000,000, Am. Geogr. Soc., New York, 1971.

Davies, G., Review of oceanic and global heat flow estimates, *Rev. Geophys.*, *18*, 718–722, 1980.

Denlinger, R. P., A revised estimate for the temperature structure of the oceanic lithosphere, *J. Geophys. Res.*, *97*, 7219–7222, 1992.

Hager, B. H., R. W. Clayton, M. A. Richards, R. P. Comer, and A. M. Dziewonski, Lower mantle heterogeneity, dynamic topography and the geoid, *Nature*, *313*, 541–545, 1985.

Herron, E. M., J. F. Dewey, and W. C. Pitman III, Arctic Ocean: Plate tectonics model for the evolution of the Arctic, *Geology*, *2*, 377–380, 1974.

Horai, K., and G. Simmons, Spherical harmonic analysis of terrestrial heat flow, *Earth Planet. Sci. Lett.*, *6*, 386–394, 1969.

Jackson, H. R., and K. Gunnarson, Reconstruction of the Arctic: Mesozoic to present, *Tectonophysics*, *172*, 303–322, 1990.

Jackson, M. J., H. N. Pollack, and S. T. Sutton, On the distribution of anomalous mass within the Earth: Forward models of the gravitational potential spectrum using ensembles of discrete mass elements, *Geophys. J. Int.*, *107*, 83–94, 1991.

Jessop, A. M., M. A. Hobart, and J. G. Sclater, The world heat flow data collection—1975, *Geotherm. Ser. 5*, 125 pp., Earth Phys. Branch, Ener., Mines and Resourc., Ottawa, Canada, 1976.

Kumazawa, M., and O. L. Anderson, Elastic moduli, pressure derivatives, and temperature derivatives of single-crystal olivine and single-crystal forsterite, *J. Geophys. Res.*, *74*, 5961–5972, 1969.

Lachenbruch, A. H., and J. H. Sass, Heat flow and the thermal regime of the crust, in *The Earth's Crust, Its Nature and Physical Properties, Geophys. Monogr. Ser.*, vol. 20, edited by J. G. Heacock, pp. 625–675, AGU, Washington, D. C., 1977.

Langel, R. A., International Geomagnetic Reference Field 1991 revision, International Association of Geomagnetism and Aeronomy (IAGA) Division V, Working Group 8: Analysis of the main field and secular variation, *Geophysics*, *57*, 956–959, 1992.

Larson, R. L., W. C. Pitman III, X. Golovchenko, S. C. Cande, J. F. Dewey, W. F. Haxby, and J. L. LaBreque, The bedrock geology of the world, scale 1:23,200,000 at equator, W. H. Freeman, New York, 1985.

Lee, W. H. K., Heat flow data analysis, *Rev. Geophys.*, *1*, 449–479, 1963.

Lee, W. H. K., On the global variations of terrestrial heat-flow, *Phys. Earth Planet. Inter.*, *2*, 332–341, 1970.

Lee, W. H. K., and S. Uyeda, Review of heat flow data, in *Terrestrial Heat Flow, Geophys. Monogr. Ser.*, vol. 8, edited by W. H. K. Lee, pp. 87–100, AGU, Washington, D. C., 1965.

Lister, C. R. B., On the thermal balance of a midocean ridge, *Geophys. J. R. Astron. Soc.*, *26*, 515–535, 1972.

Louden, K. E., Marine heat flow data listing, in *Handbook of Seafloor Heat Flow*, edited by J. A. Wright and K. E. Louden, Appendix B, pp. 325–485, CRC Press, Boca Raton, Fla., 1989.

Marsh, J. G., et al., The GEM-T2 gravitational model, *J. Geophys. Res.*, *95*, 22,043–22,072, 1990.

Nyblade, A., and H. N. Pollack, A comparative study of parameterized and full thermal convection models in the

interpretation of heat flow from cratons and mobile belts, *Geophys. J. Int.*, *113*, 747–751, 1993.

Parker, R. L., and L. Shure, Efficient modeling of the Earth's magnetic field with harmonic splines, *Geophys. Res. Lett.*, *9*, 812–815, 1982.

Parsons, B., and J. G. Sclater, An analysis of the variation of ocean floor bathymetry and heat flow with age, *J. Geophys. Res.*, *82*, 803–827, 1977.

Pollack, H. N., and D. S. Chapman, On the regional variation of heat flow, geotherms, and lithospheric thickness, *Tectonophysics*, *38*, 279–296, 1977.

Pollack, H. N., and J. H. Sass, Thermal regime of the lithosphere, in *Handbook of Terrestrial Heat-Flow Density Determination*, edited by R. Haenel, L. Rybach, and L. Stegena, pp. 301–308, Kluwer Academic, Norwell, Mass., 1988.

Revelle, R., and A. E. Maxwell, Heat flow through the floor of the eastern North Pacific Ocean, *Nature*, *170*, 199–200, 1952.

Rona, P., K. Bostrom, L. Laubier, and K. Smith, Jr. (Eds.), *Hydrothermal Processes at Seafloor Spreading Centers*, 796 pp., Plenum, New York, 1983.

Sclater, J. G., and J. Francheteau, The implication of terrestrial heat flow observations on current tectonic and geochemical models of the crust and upper mantle of the Earth, *Geophys. J. R. Astron. Soc.*, *20*, 509–542, 1970.

Sclater, J. G., J. Crowe, and R. N. Anderson, On the reliability of oceanic heat flow averages, *J. Geophys. Res.*, *81*, 2997–3006, 1976.

Sclater, J. G., C. Jaupart, and D. Galson, The heat flow through oceanic and continental crust and the heat loss of the Earth, *Rev. Geophys.*, *18*, 269–311, 1980.

Sprague, D., and H. N. Pollack, Heat flow in the Mesozoic and Cenozoic, *Nature*, *285*, 393–395, 1980.

Stein, C., and S. Stein, A model for the global variation in oceanic depth and heat flow with lithospheric age, *Nature*, *359*, 123–129, 1992.

Su, W., R. L. Woodward, and A. M. Dziewonski, Deep origin of mid-ocean-ridge seismic velocity anomalies, *Nature*, *360*, 149–152, 1992.

Williams, D. L., and R. P. von Herzen, Heat loss from the Earth: New estimate, *Geology*, *2*, 327–328, 1974.

Williams, D. L., R. P. von Herzen, J. G. Sclater, and R. N. Anderson, The Galapagos spreading center: Lithospheric cooling and hydrothermal circulation, *Geophys. J. R. Astron. Soc.*, *38*, 587–608, 1974.

S. J. Hurter, Institute of Astronomy and Geophysics, University of São Paulo, São Paulo SP CEP 01065 Brazil.

J. R. Johnson, Department of Geosciences, University of Arizona, Tucson, AZ 85721.

H. N. Pollack, Department of Geological Sciences, University of Michigan, Ann Arbor, MI 48109-1063.